The Eurasia Proceedings of Science, Technology, Engineering & Mathematics (EPSTEM)
ISSN: 2602-3199

The Eurasia Proceedings of Science, Technology, Engineering and Mathematics (EPSTEM), 2025

Volume 37, Pages 790-810

ICEAT 2025: International Conference on Engineering and Advanced Technology

Numerical Analysis of Perforation Steel Plates Impacted by Blunt, Conical, Hemispherical, and Spherical Projectiles

Baneen Qasim Kazem
University of Al-Qadisiyah

Muhanad Hamed Mosa
University of Al-Qadisiyah

Abstract: Penetrating mechanics was developed for military applications and has been applied in the design and production of bulletproof plates, protective armor, warships, and heavy military vehicles. However, the perforated plates are considered a contemporary type of structure. Hence, the issue is about the extent of the effect of perforation of panels on ballistic performance. The impact of different projectile forms on two types of thin steel plates—perforated and non-perforated panels is examined numerically in this paper. The ABAQUS-Explicit finite element system was utilized for numerical simulations, and the perforation process was accurately estimated using the Johnson-Cook fracture criterion. Indeed, all projectile shapes, whether blunt, conical, hemispherical, or spherical, are designed and modeled with wide impact velocities between 200 to 500 m/s. This work takes into consideration plastic properties, the temperature differential created in the plate, and adiabatic shear bands. They concluded, through numerical analysis, that perforated panels can be considered a promising option for use as armor due to several considerations, the most important of which is energy savings as a result of reducing density.

Keywords: Perforated panels, Ballistic impact, Finite element method, Johnson-cook model, ABAQUS

Introduction

The way materials behave under dynamic loading is of great importance, especially when it comes to penetration and perforation caused by the impact of non-deformable projectiles (Ibrahim et al., 2014). Impact on panels is a complex and wide-ranging issue involving friction, contact, breakage, and wear. Large plastic deformation at high strain rates, dynamic plastic flow, elastic and plastic wave propagation, and kinetic energy transfer are all irreversible thermodynamic processes induced by internal energy (Arias et al., 2008; Mosa & Hamzah, 2022). Previous studies have focused on plates within a specific thickness range, affected by projectiles with a particular nose shape within a certain velocity range. However, several studies have shown that the deformation and failure patterns of sheet metal vary depending on the impact velocity, the shape of the projectile nose, and the ratio of the projectile diameter to the sheet thickness(Chen et al., 2017; Mosa et al., 2024; Rusinek et al., 2009). Additional research has highlighted the impact of plate thickness and projectile form.

In this work, a numerical analysis was performed to study the maximum impact force and deformation characteristics of a steel plate subjected to spherical, hemispherical, blunt, and conical projectiles. The projectile impact velocity ranged from 200 to 500 m/s. Numerical simulations were performed using ABAQUS/Explicit software with the Johnson-Cook (JC) calibrated model for flexible-viscous-plastic materials(Senthil et al., 2018).

Using various projectiles, target performance was evaluated using three sets of Johnson-Cook coefficients. The results for force, deflection, and target breaking were compared using a target thickness of 3 mm. The Finite Element Method (FEM) has been widely employed to simulate ballistic impact events, emphasizing its importance. The process analysis in this study assumes the following assumptions: (a) absorption of projectile energy, (b) the plastic deformation of the target plate is considered, while the elastic deformation is ignored. This work aims to compare the compatibility of each type of projectile using numerical methodology through ABAQUS software. As a result, this research highlights the program's ability to identify different responses to a wide range of complex ballistic impact studies. Furthermore, this research presents the results of a numerical study conducted to analyze the perforation process of different projectile shapes and speeds with two types of targets, perforated and non-perforated panels.

Geometry and Material Properties

Projectiles have various properties that affect their function and performance. Two basic properties, hardness and flexibility, are necessary to maintain the forces after a ballistic impact. The behavior of a projectile is greatly influenced by the composition of the material, which is usually steel. The research available in the international literature covers a large part of the behavior of high-strain-rate metallic materials in various engineering applications.(Ibrahim et al., 2014; Ekrami et al., 2017; Reck et al., 2022). On the other hand, parameters such as radius and length influence stability and penetration strength. Further, the projectile's trajectory is also affected by the change in mass and final ballistic impact performance. The specifications of spherical and hemispherical projectiles, as well as blunt and conical projectiles, include various specific aspects. Figure 1 shows the size and shape of the projectiles, and the mechanical properties of the projectile materials are shown in Table 1

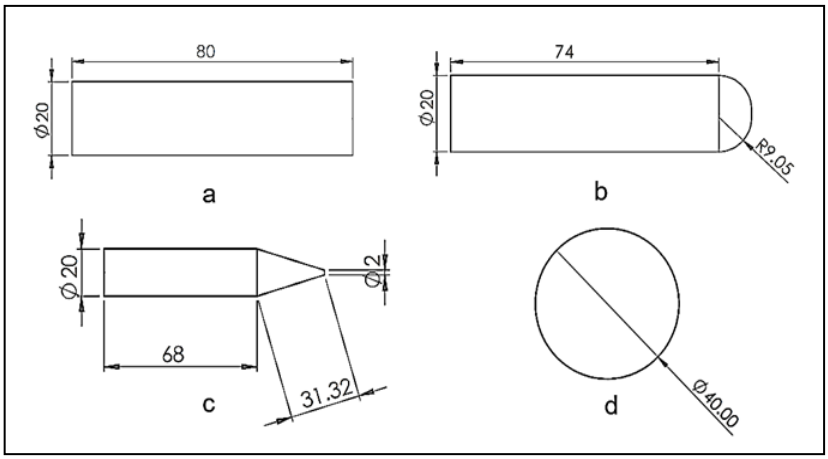

Figure 1. Geometrical dimensions for four types of projectiles
(a) Blunt (b) Hemispherical (c) Conical (d) Spherical

Table 1. Mechanical and physical properties of projectiles

Modulus of Elasticity (GPa)	Poisson Ratio	Density (kg/m^3)
200	0.33	7800

Metals have several important properties, including strong tensile strength, toughness, ductility, and a high yield point. However, due to high density, this material should not be utilized much despite its important qualities. There are two types of panels employed in this work: the non-perforated steel panel and the perforated steel panel. Using two different types of panels allows comparison of the panels and helps to understand the benefits of this type of panel. However, the numerical study modelled monolithic steel plates, and the dimensions of each plate are 200×200 mm, with a 3mm plate thickness. The size and appearance of the panel are shown in Figure 2. The mechanical characteristics of the panel materials are given in Table 2.

Table 2. Mechanical and physical properties of Perforated and Non-perforated steel panels

Modulus of Elasticity (GPa)	Poisson Ratio	Density (kg/m^3)
200	0.33	7800

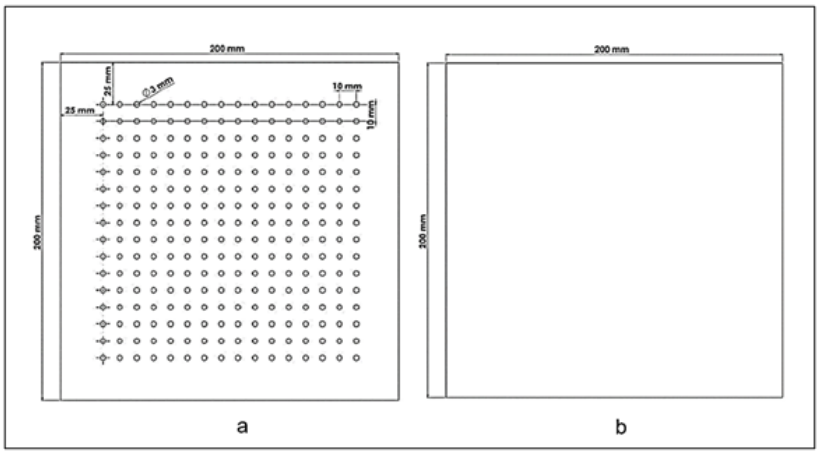

Figure 2. The geometry and dimensions of different types of plates
(a) Perforated steel panel (b) non-perforated steel panel

Numerical Modeling with ABAQUS

The finite element model of the projectile was created using 3D modeling technology in ABAQUS software, a well-known program that uses the finite element method to study how a body reacts to static and dynamic stresses. A 3D hexahedron mesh was used to illustrate this projectile, as shown in Figure 3

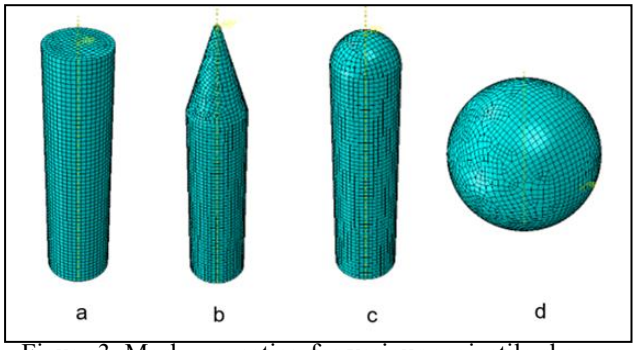

Figure 3. Mesh generation for various projectile shapes:
(a) Blunt (b) Conical (c) Hemispherical (d) Spherical

First, the process involves creating a quadrilateral mesh using the 2D Mesh tool in the ABAQUS software. The preceding 2D mesh is then rotated along the edge's axis to create a 3D mesh with a hexahedral mesh form. Model organization is a critical issue to consider in the FE Explicit (Dynamics) program because it affects the duration of the simulation analysis. For this research, the space between the projectile and target face is zero; thus, the projectile and target will be in direct contact when the simulation begins. The reason for specifying this distance is to reduce the time required to simulate the process. (Oudah et al., 2023; Sun et al., 2018). The model established for the blunt and hemispherical, conical, and spherical projectile before impacting on the target is shown in Figure 4. Table 3 depicts the total number of nodes and elements of the projectiles.

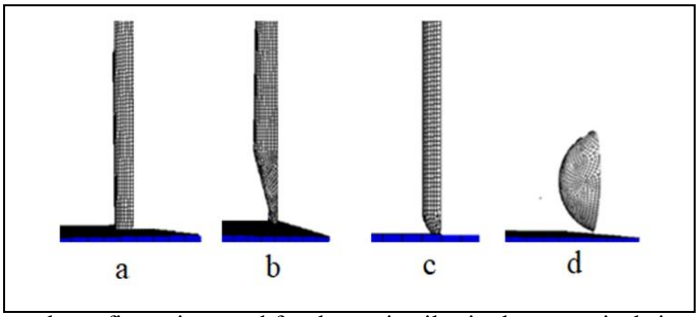

Figure 4. The mesh configuration used for the projectiles in the numerical simulation
Blunt (b) Conical (c) Hemispherical (d) Spherica

Table 3. Total number of projectile elements and nodes

Type	Elements Numbers	Nodes Numbers
Blunt	2980	2974
Hemispherical	2950	2940
Conical	3160	3139
Spherical	3043	2997

To simulate the steel plate piercing process, researchers created a 3D Lagrangian finite element model using ABAQUS/Explicit. The fully three-dimensional configuration of the model allows for the illustration of the radial cracking and petal failure process, which describes the behavior of blunt, hemispherical, conical, and spherical projectiles in metal plates(Rodríguez-Martínez et al., 2013; Dubey et al., 2021; Alobaidi et al., 2023; Mosa & Hamza, 2022). A sensitivity analysis was utilized to select the mesh arrangement. It provides findings about the energy absorbed by the target regardless of the mesh density. The upcoming section of the article will illustrate this. The viscoplastic technique used to evaluate material behavior enhances mesh-independent findings.

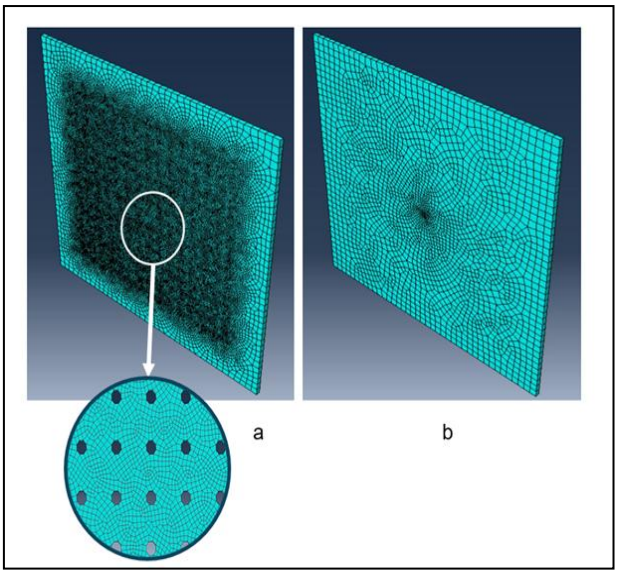

Figure 5. A model that uses the finite elements of two types of plates
(a) Perforated steel panel (b) non-perforated steel panel

Mesh-dependent strain softening issues in plasticity can be solved via the regularization process of viscoplasticity.(Tang & Li, 2022;Alobaidi & Almuramady, 2022). To define the mesh of monolithic structure for non-perforated and perforated steel panels, to construct this mesh, a basic tool. Due to the simple structure of the steel plates, A hexahedron mesh was created using the quadrilateral mesh. The metal target was made after selecting the number of elements in each direction (x, y, z). The ABAQUS software was used to create the element shapes and the metal sheet networks. The hexahedron mesh for the metal plate is shown in Figure 5, along with form meshes created with ABAQUS software. Each panel's total elements and nodes are displayed in Table 4.

Table 4. Number of elements and nodes for perforated and non-perforated steel panel

Type	Elements Numbers	Nodes Numbers
Perforated steel panel	24209	50116
Non-perforated steel panel	2892	5946

Constitutive Model

The theory of contact deformation can be applied to relate the normal contact force, and then relate the deformation to the work done on the contact area by the normal force of the colliding bodies. This research used a 3-dimensional solid projectile that collided with an elastic-plastic target plate. To investigate the problem, an explicit nonlinear 3D finite element software was used. In plastic elastic contact, the transition between elastic and plastic behavior can depend on the stress field by expanding a cylindrical or spherical cavity in a plastic

elastic solid. Based on the results, which showed no wear on the projectile surface upon contact, the projectile was characterized as a solid body. The computing time required for simulations decreases with this assumption. A constant value of 0.1 of the Coulomb friction coefficient1 was employed to specify where the bullet impacts the plate. The steel plate is made of mechanically heat-rolled ferrous structural steel, which has great ductility and strength. $\bar{\varepsilon}^P \approx 1$ The yield stress is $\sigma_y \approx 500\ Mpa$, while the failure stress $\bar{\sigma}_{failure} \geq 1Gpa$. This material was chosen because of its extensive research and published experimental results on tension and perforation. It allows the confirmation of numerical findings (Rusinek et al., 2009; Mansour et al., 2016). Thermo-viscoplastic behavior can be defined analytically using physical or phenomenological approaches. Furthermore, the phenomenological approach emphasizes several essential relations (Senthil et al., 2018; Salimi et al., 2022). Since the Johnson-Cook (JC) model is sensitive to high strain rates, it has thermal softening, large deformation, and ductile behavior at high impact velocities. Additionally, this form is already prepared in ABAQUS-Explicit. The following is an explicit appearance of the Johnson-Cook model:

$$\bar{\sigma}(\bar{\varepsilon}^P, \dot{\bar{\varepsilon}}^P, T) = [C_1 + C_2(\bar{\varepsilon}^P)^n]\left[1 + C_3 \ln\left(\frac{\dot{\bar{\varepsilon}}^P}{\dot{\varepsilon}_0}\right)\right][1 - T^{*m}] \qquad (1)$$

C1 indicates the yield stress, C2 is a material constant, n is the hardening parameter, C3 is the strain rate sensitivity, and m is the temperature sensitivity parameter. $\dot{\varepsilon}_0$The constitutive relation lower limit and the homologous temperature are $T^* = (T - T_0)/(T_m - T_0)$ T the current temperature and T_0 Is the ambient temperature, as well as T_m, the melting temperature, Table 5. Shows the JC model constant (Rodríguez-Martínez et al., 2013; Alawsi et al., 2025; Ghazlan et al., 2023).

Table 5. Johnson-Cook model constant

C_1	C_2	C_3	*n*	*m*	T_m *(k)*
490	807	0.012	0.73	0.94	1800

Model of Fracture

A failure condition must be applied to model the perforation process using a Lagrangian framework. When studying metallic structures under dynamic stress, the failure criteria can be used to evaluate material deformation behavior(Alobaidi & Almuramady, 2023)Coppinger et al., 2022). Material failure is expressed using a constant plastic stress value. The tension along the bullet and plate remains constant during the piercing process because the target is so thin. The value of the failure stress in the simulation, f = 0.50, is determined by experimentally measuring the deformation behavior of the material. This value is slightly greater than the necking strain that occurred during dynamic loading. The finite element simulation provides a sufficient description of the strain location and necking process that causes plate perforation(Ibrahim et al., 2014),(Mosa & Hamza, 2022).

The fracture model applied in this research is an extension of the criteria introduced by Hancock and MacKenzie(1976). Johnson and Cook suggested that the formula, D parameter, can be calculated by summing all deformation increments. To incorporate strain $\bar{\boldsymbol{\varepsilon}}^{\boldsymbol{P}}$ strain rate $\dot{\bar{\boldsymbol{\varepsilon}}}^{\boldsymbol{P}}$, and temperature (T) dependence. This model incorporates stress triaxiality (σ*), an essential property for this type of application. When parameter D exceeds unity, it is assumed to fail. The D parameter indicated the total of all deformation increments. The development of D is as follows(Ashaari et al., 2020; Chen et al., 2023). The following is D's development:

$$D(\bar{\varepsilon}^p, \dot{\bar{\varepsilon}}^p, T, \sigma^*) = \sum\left(\frac{\Delta\bar{\varepsilon}^p}{\bar{\varepsilon}_f^p(\dot{\bar{\varepsilon}}^p, T, \sigma^*)}\right) \qquad (2)$$

In this equation $\Delta\bar{\varepsilon}^P$, represents the cumulative equivalent plastic strain over an integration cycle, whereas represents the critical failure strain $\bar{\varepsilon}^P$. The plastic failure strain $\bar{\varepsilon}^p$ is determined by a non-dimensional plastic strain rate$\dot{\bar{\varepsilon}}^p/\dot{\varepsilon}_0$ a dimensionless pressure-deviatoric stress ratio $\sigma^* = \sigma_m/\bar{\sigma}$ The mean stress $\sigma_m$and equivalent stress $\bar{\sigma}$. and a non-dimensional temperature (T*) as previously defined. The dependencies are $\bar{\varepsilon}^p = f(\sigma^*.\dot{\bar{\varepsilon}}^p.T)$ believed to be separable and can be expressed as follows (Arias et al., 2008),(Ekrami et al., 2017),(Chen et al., 2021). Table 6. Shows the JC fracture model constant.

$$\begin{cases} \bar{\varepsilon}_f^p = [D_1 + D_2 exp(D_3\sigma^*)]\left[1 + D_4 \ln\left(\frac{\dot{\bar{\varepsilon}}^p}{\dot{\varepsilon}_0}\right)\right][1 + D_5 T^*] \\ \sigma^* = \frac{1}{3\bar{\sigma}}(\sigma_1 + \sigma_2 + \sigma_3) \end{cases} \quad (3)$$

Table 6. Johnson-Cook fracture model constant

D_1	D_2	D_3	D_4	D_5
0.0705	1.732	-0.45	0.00123	0.94

Impact Location of the Perforated Plate

Because the perforated plate featured various locations where the bullet may impact, and therefore deciding the site of the shot's fall lends credibility and realism to scientific investigation, the place of the shot was chosen as indicated in Figure 6.

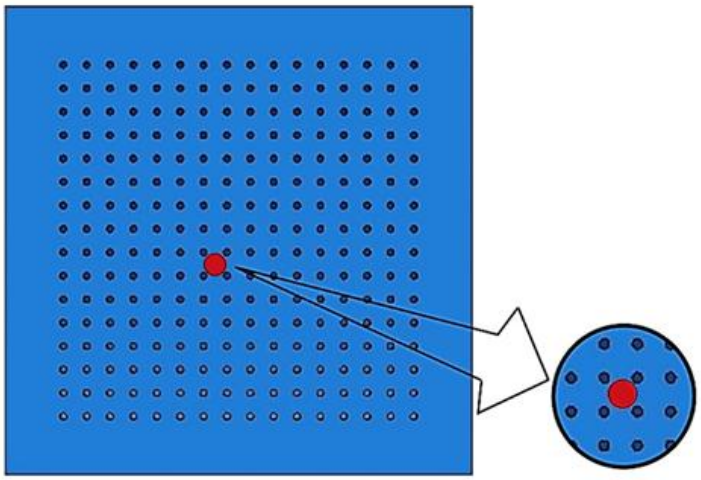

Figure 6. Numerical modelling of perforated plate process, red circle. Refer to the location of the impact of the projectile

Results and Analysis

After conducting numerical simulations, the values of the residual velocities after the collision were determined for both perforated and non-perforated panels. The results showed that perforating the panels does not generally affect the panels' resistance to projectiles. The figure shows the velocities before and after perforating the panels. Figure 7 depicts the comparison between different types of projectiles' nose to an initial and residual velocity for perforated and non-perforated plates.

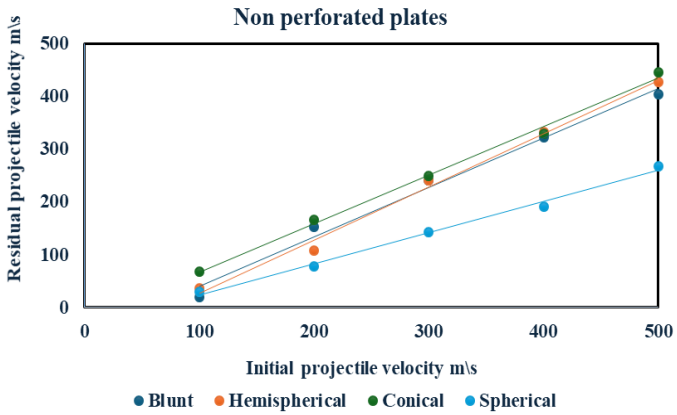

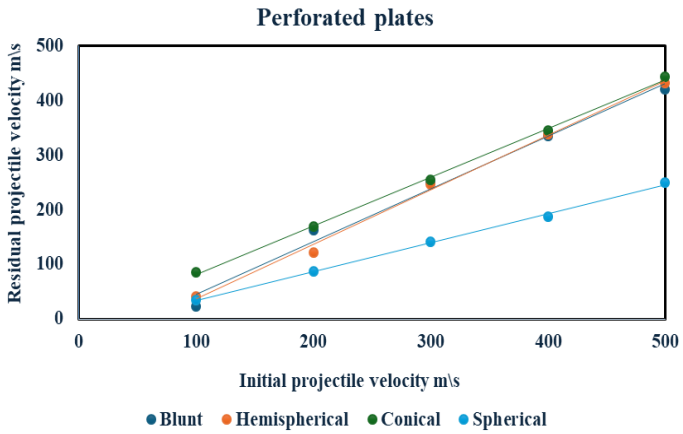

Figure 7. Comparison between different types of projectiles according to an initial and Residual velocity for two types of plates (perforated and non-perforated)

Table 7 indicates the results of the residual velocity of different types of projectiles and initial velocity for non-perforated plates. From this table, the results show that the maximum residual velocities are for the conical projectile, and the minimum value of residual velocities is for the blunt projectile.

Table 7. Results of the residual velocity of different types of projectiles for non-perforated plates

	Blunt	Hemspherical	Conical	spherical
Vi	Vr	Vr	Vr	Vr
100	19.7191	36.8281	67.7977	30.029
200	153.294	107.685	166.11	78.1639
300	241.163	240.574	249.814	142.969
400	322.898	333.465	328.558	191.261
500	403.654	426.653	445.396	267.677

Table 8 indicates the results of the residual velocity of different types of projectiles and initial velocity for perforated plates. From this table, the results show the maximum residual velocities for the conical projectile, and the minimum value of residual velocities is for the blunt projectile.

Table 8. Results of the residual velocity of different types of projectiles for perforated plates

	Blunt	Hemspherical	Conical	spherical
Vi	Vr	Vr	Vr	Vr
100	23.0895	41.8891	85.1499	35.0686
200	162.36	121.527	169.83	86.807
300	249.179	246.259	254.167	140.56
400	335.041	337.715	344.125	186.742
500	419.758	432.153	443.688	250.29

Table 9 indicates the results of the deviation of residual velocity of different types of projectiles and initial velocity for perforated plates. From this table, the results show that the maximum deviation of residual velocities is for the conical projectile, and the minimum deviation of residual velocities is for the blunt projectile.

Table 9. Deviation of residual velocity (Pd) values between perforated and non-perforated plates

	Blunt	Hemspherical	Conical	spherical
Percent of deviation of residual velocity %				
Vi	Pd %	Pd %	Pd %	Pd %
100	17%	14%	26%	17%
200	6%	13%	2%	11%
300	3%	2%	2%	2%
400	4%	1%	5%	2%
500	4%	1%	0%	6%

Blunt Projectile

Figure 8 illustrates the time sequence of the blunt projectile impact on the non-perforated plate for two impacted velocities, 200 m/s and 500 m/s. This figure represents the behavior of the panel after the collision, as well as the failure pattern.

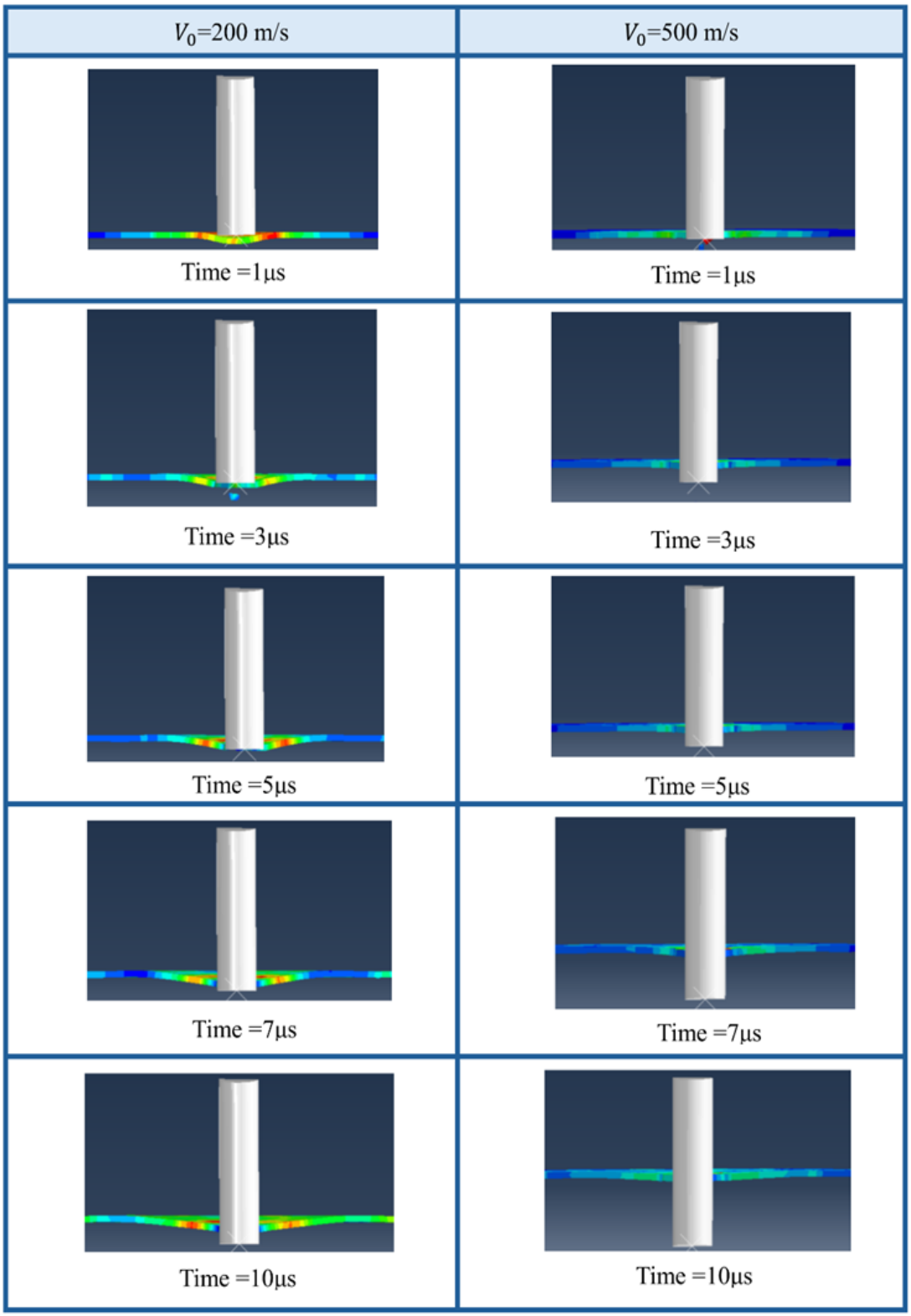

Figure 8. Deformation behaviour of a non-perforated plate impacted by a blunt projectile.
Left: Vo = 200 m/s; Right: Vo = 500 m/s

Figure 9 demonstrates the graph simulation of a perforated plate subjected to a blunt projectile at two distinct speeds, :

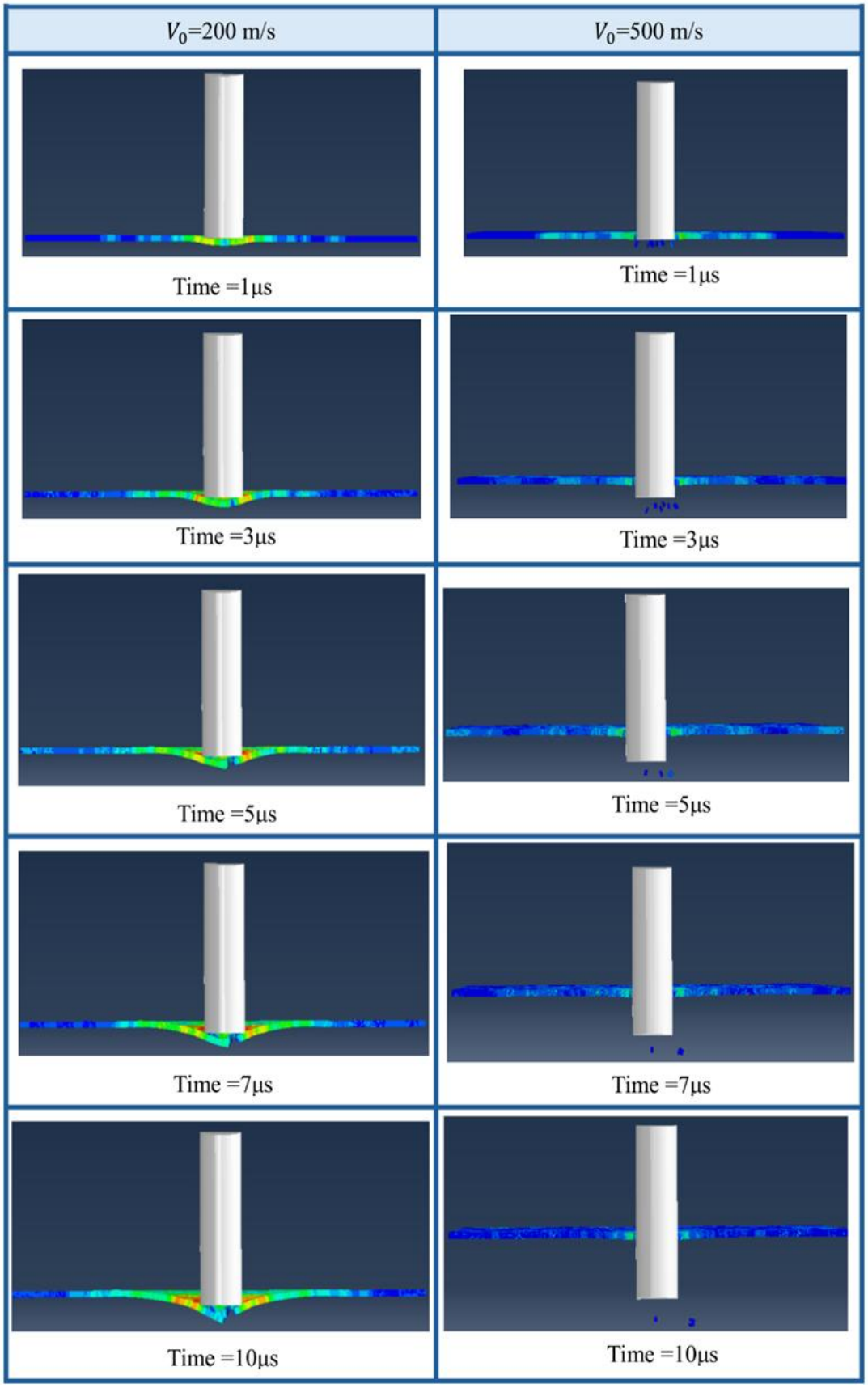

Figure 9. Numerical simulation of the perforated plate process for a blunt projectile.
Left: Vo = 200 m/s; Right: Vo = 500 m/s, location B

Hemispherical Projectile

Figure 10 displays the simulation results for the non-perforated plate exposed to the impact of a hemispherical projectile at two impacted velocities: 200 m/s and 500 m/s. This figure illustrates the behavior of the panel after the effects and the failure mode.

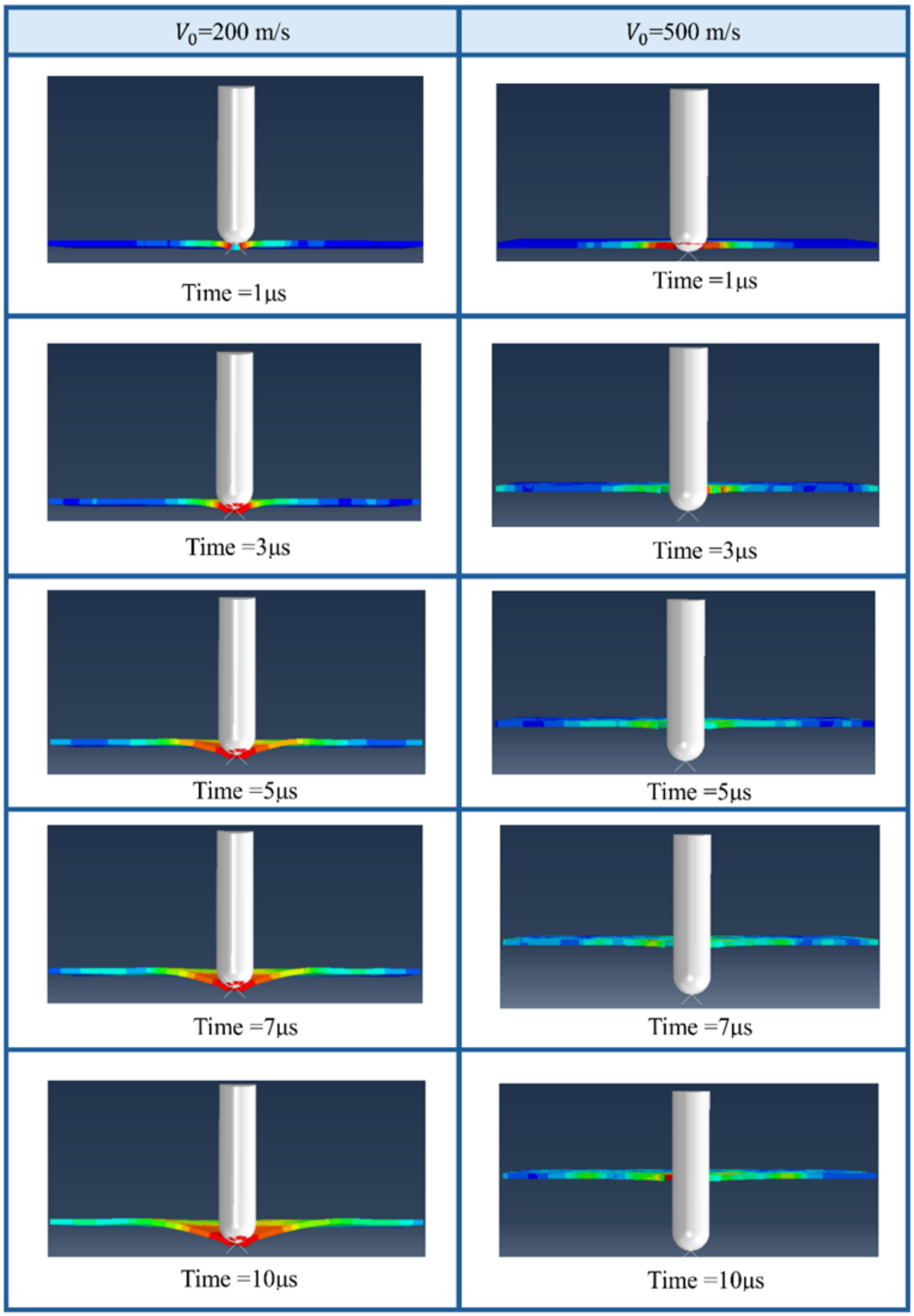

Figure 10. The non-perforated plate for hemispherical projectiles is numerically simulated.Left: Vo = 200 m/s; Right: Vo = 500 m/s

Figure 11 shows the time sequence of the hemispherical projectile hitting the perforated plate for two types of impacted velocities, 200 m/s and 500 m/s. This figure illustrates the plate behaviour after the impact and the failure mode.

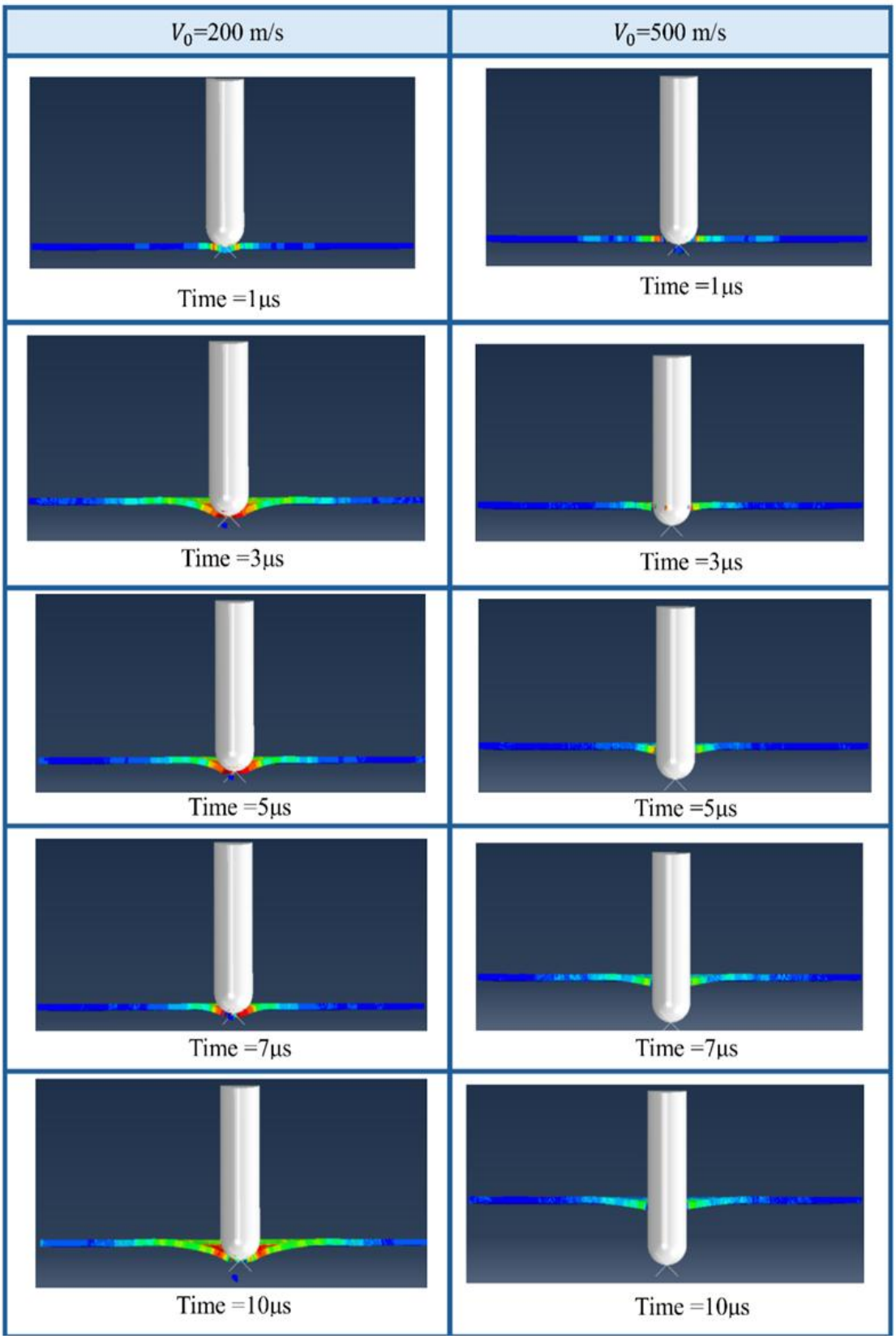

Figure 11. Numerical modeling of a hemispherical projectile using a perforated plate technique. Left: Vo = 200 m/s; Right: Vo = 500 m/s, location B

Conical Projectile

Figure 12 shows the time sequence of the conical projectile impact on the non-perforated plate for two types of impacted velocities, 200 m/s and 500 m/s. This figure illustrates the behavior of the plate after the impact and the failure mode.

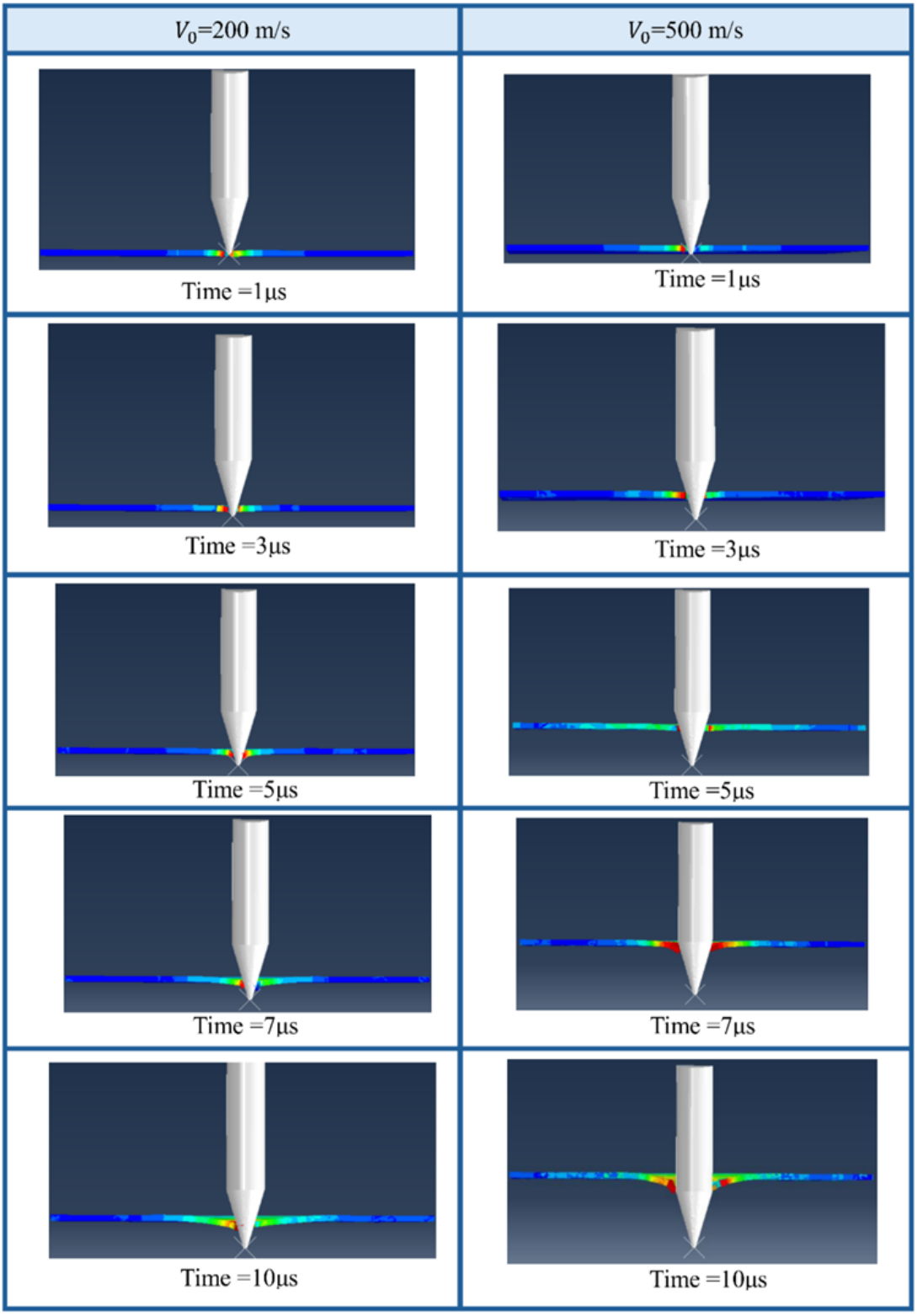

Figure 12. Failure mode of the non-perforated plate process for a conical projectile.
Left: Vo = 200 m/s; Right: Vo = 500 m/s

Figure 13 shows the time sequence of the conical projectile impact on the perforated plate for two types of impacted velocities, 200 m/s and 500 m/s. This figure illustrates the behavior of the plate after the impact and the failure mode.

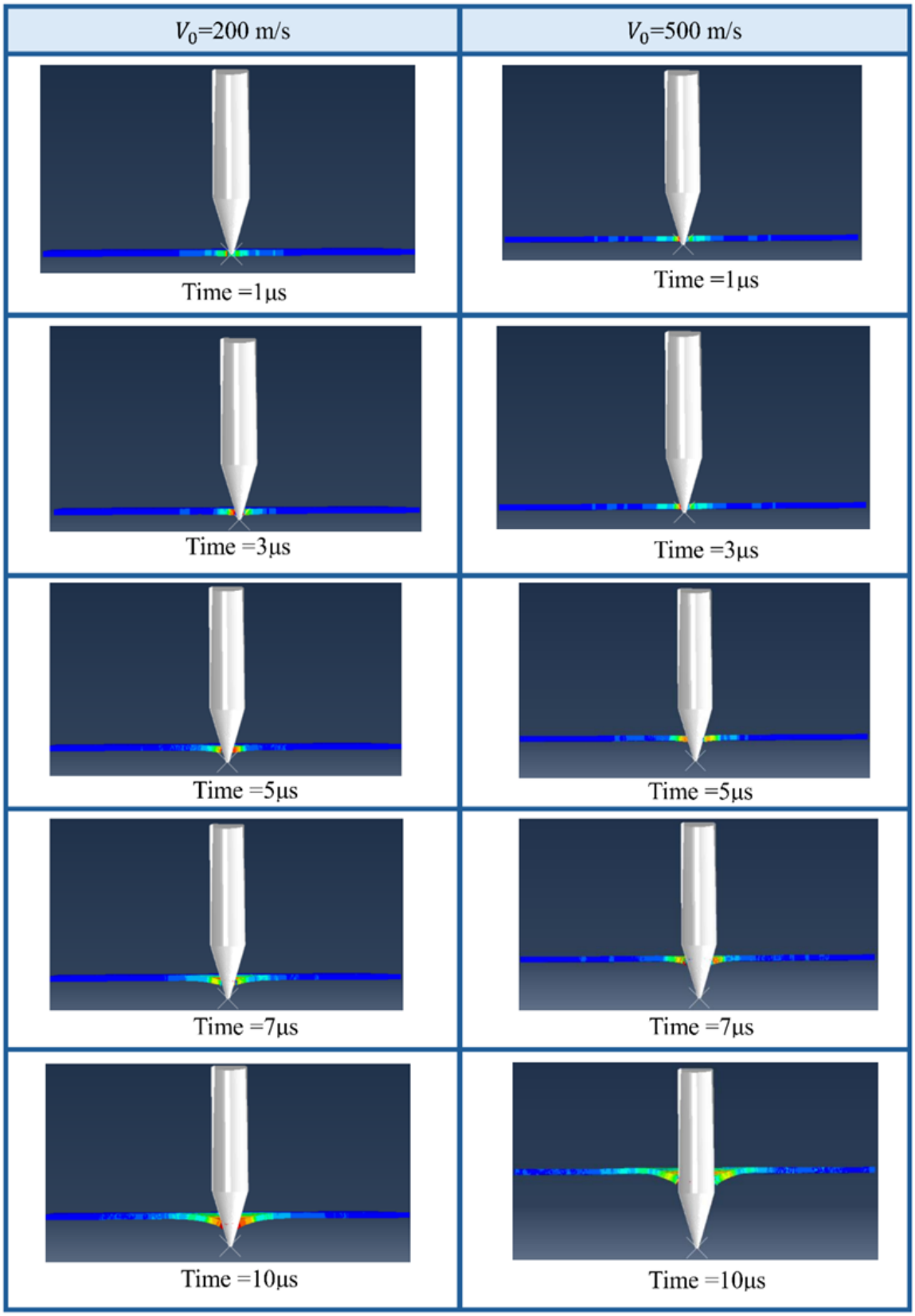

Figure 13. The simulation result of the perforated plate process for a conical projectile.
Left: Vo = 200 m/s; Right: Vo = 500 m/s, location B

Spherical Projectile

Figure 14 shows the time sequence of the spherical projectile impact on the non-perforated plate for two types of impacted velocities, 200 m/s and 500 m/s. This figure illustrates the behavior of the plate after the impact and the failure mode

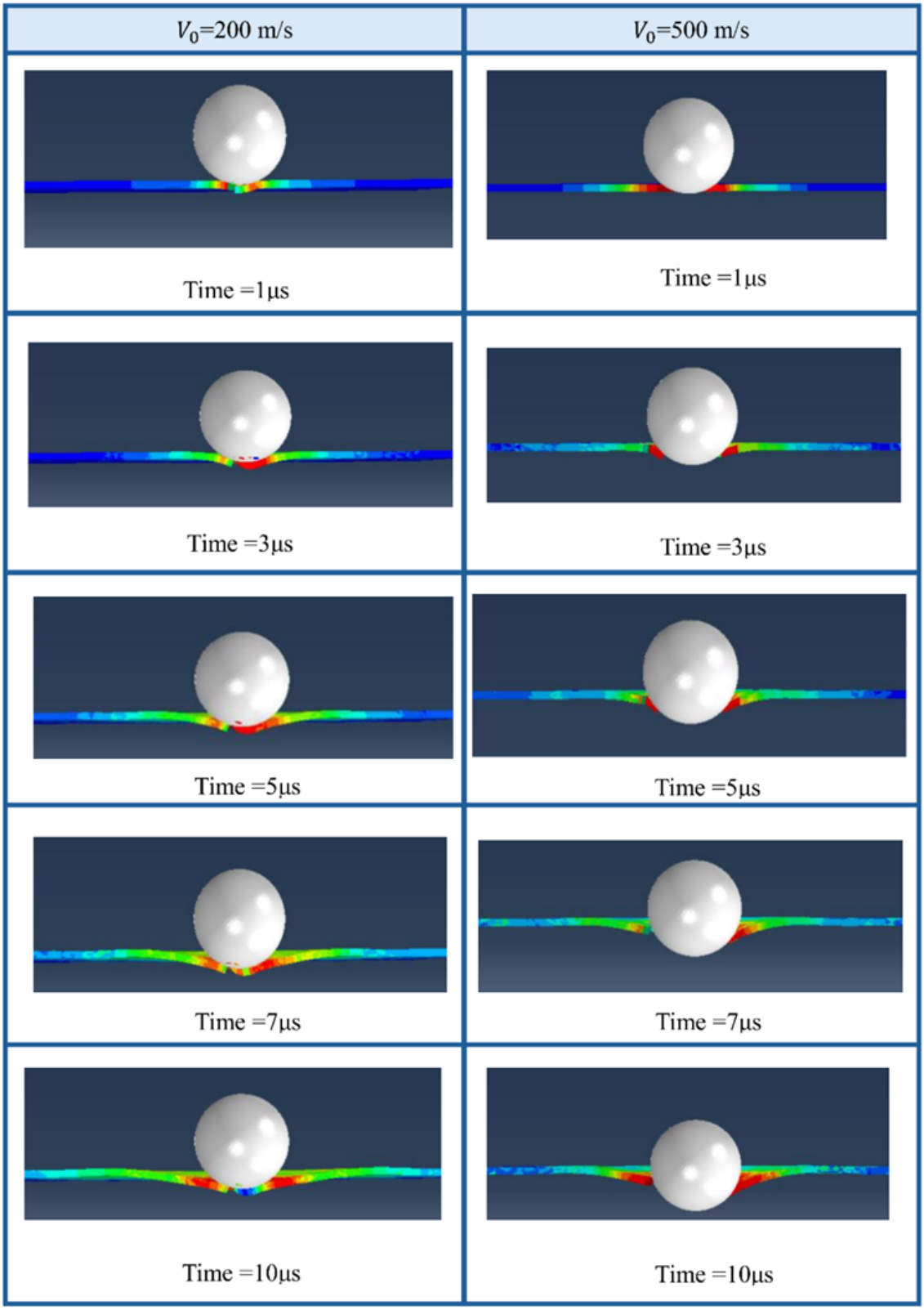

Figure 14. Simulation of the non-perforated plate process for a spherical projectile.
Left: Vo = 200 m/s; Right: Vo = 500 m/s

Figure 15 illustrates the time sequence of the impact of the spherical projectile on the perforated plate for the two types of impacted velocities, 200 m/s and 500 m/s.This figure demonstrates the failure mechanism and plate behavior upon impact

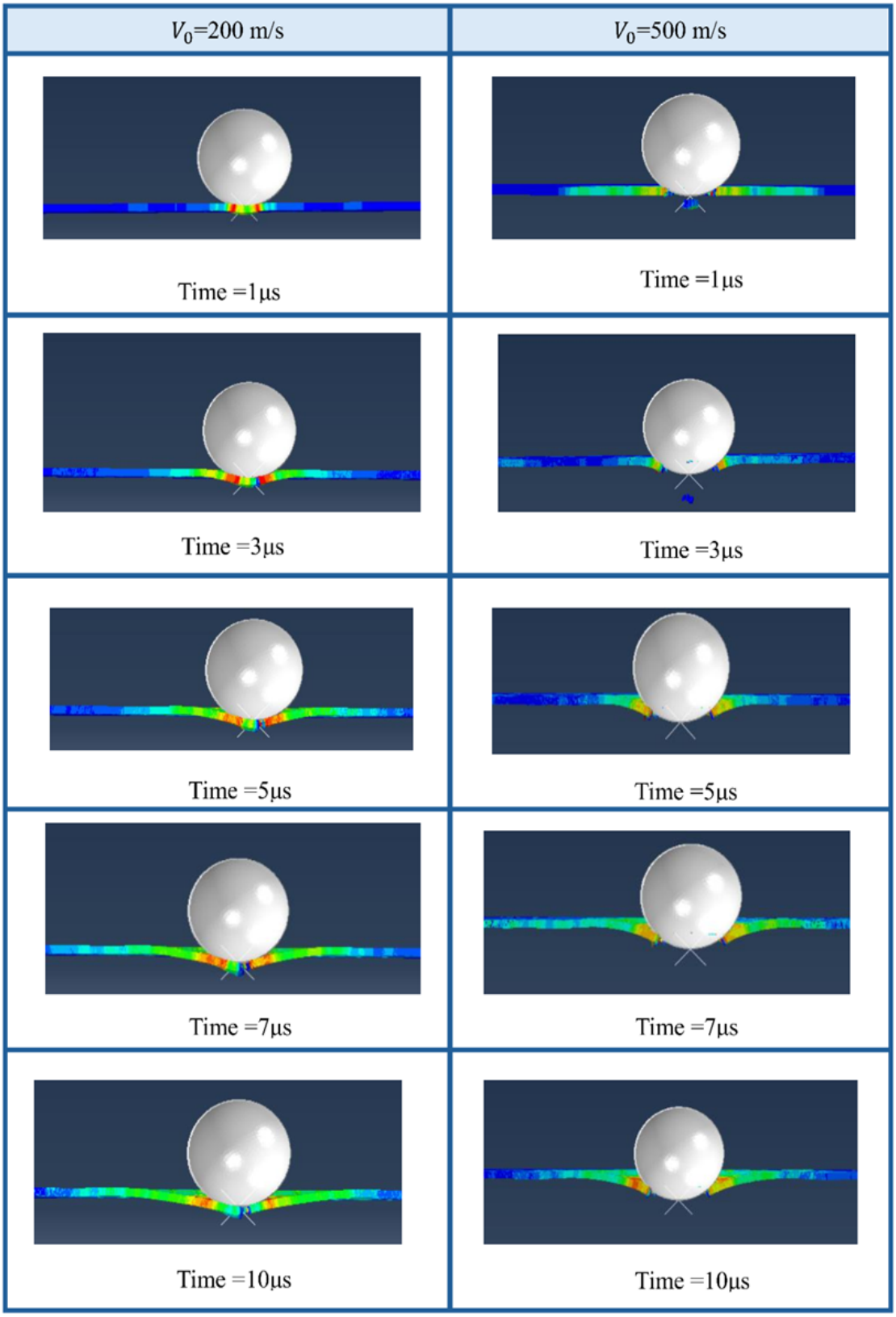

Figure 15. Ballistic penetration process of the spherical projectile in the perforated plate.
Left: Vo = 200 m/s; Right: Vo = 500 m/s

After conducting the simulation using a set of important conclusions can be reached in analyzing the behavior of the four types of projectiles (blunt, hemispherical, conical, and spherical) used in this study, which can be summarized in the following points:

Blunt Nose Projectile

- The blunt projectile has a lower residual velocity than a conical nose.
- The flat front creates higher impact resistance, causing more energy to be absorbed by the target, resulting in greater deformation or plugging.
- The blunt projectile is less effective in penetration, but better for inducing damage via blunt trauma.

Conical Nose Projectile

- The conical projectile has the highest residual velocity across all initial velocities.
- meaning they penetrate the target more effectively, retaining more of their velocity post-impact.
- The sharp point of the cone concentrates the force on a small area, promoting deeper penetration and less energy loss to the target.

Hemispherical Nose Projectile

- The hemispherical projectile performs similarly to the blunt but better in some velocity ranges.
- The curved front lowers the abrupt resistance found in blunt noses, resulting in more balanced energy dissipation and penetration.
- It still trails behind ogive and conical shapes, but maintains intermediate behavior between sharp and blunt projectiles.

Spherical Nose Projectile

- The spherical projectile has the lowest residual velocity across all velocities.
- This indicates the least efficient penetration capability.
- Its broad, rounded surface causes significant resistance upon impact, leading to petaling or extensive deformation of the plate rather than clean perforation.
- It loses more kinetic energy during the impact process, thus being less suited for deep penetration, but effective for spreading impact forces.

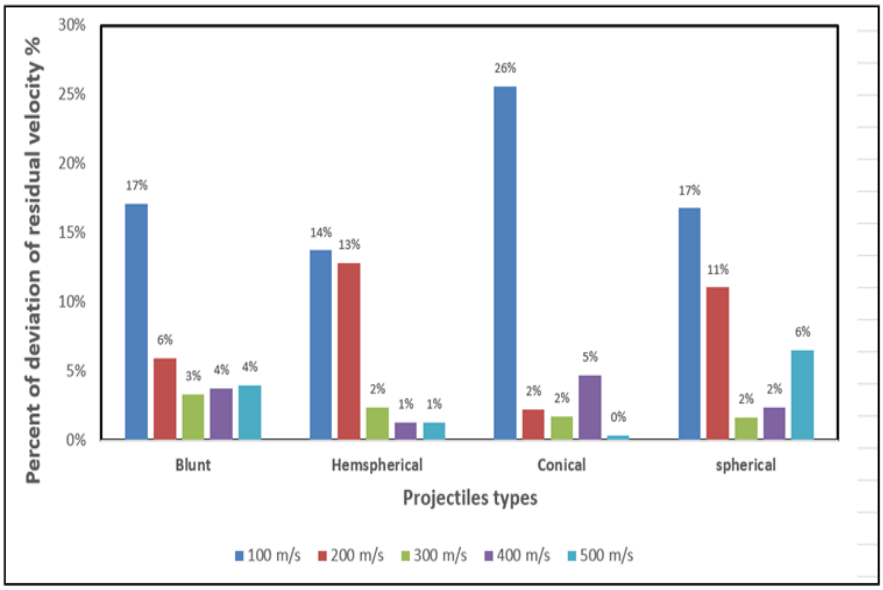

Figure 16. Comparison of the deviation of residual velocity values

As a result, the a slight difference between the residual velocities of both perforated and non-perforated plates. Subsequently, these results indicate the possibility of using perforated plates instead of non-perforated plates with high efficiency, and thus the possibility of reducing the weights of the armor by using this type of plate. Figure 16 illustrates that increasing the velocity of the projectile reduces the percentage of deviation and vice versa.

Failure Evaluation

Blunt Projectile

The failure caused by the shearing from the blunt bullet leads to the formation of a plug. The flat base makes consistent contact with the plate, concentrating stress along the edge of the contact area, which initiates shear bands. As stress increases, a circular plug shears off and is ejected from the rear, as seen in the figure. The deformation remains relatively contained, with little bending outside the shear zone. Stress is spread circumferentially, and breakdown happens when shear stress exceeds material limitations, as shown in Figure 17. This mode exhibits high-speed, localized perforation, which frequently results in smooth hole creation. The plug ejection indicates effective penetration and strong stress localization while avoiding significant surface cracking.

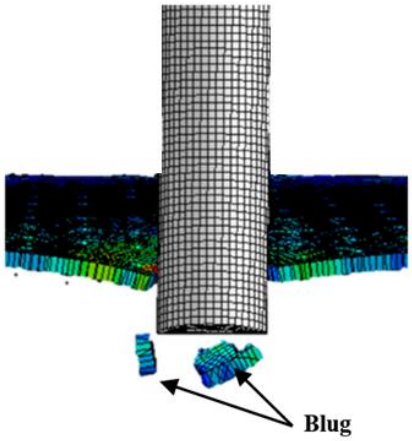

Figure 17. Simulation result for blunt projectile after impact (Section view)

Hemispherical Projectile

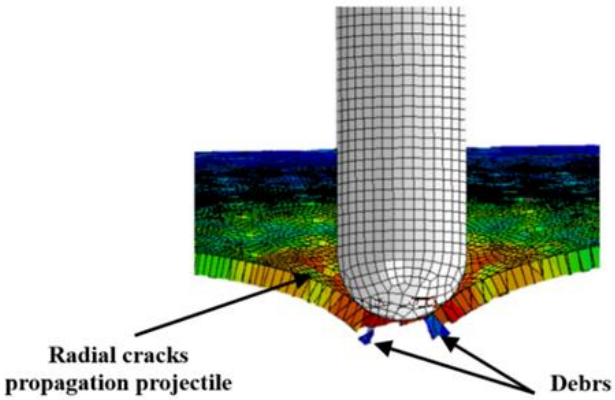

Figure 18. Simulation result for hemispherical projectile after impact (Section view)

The hemispherical projectile causes high compressive stress directly beneath the impact point, followed by radial crack propagation. The flat nose reduces penetration by sharp cutting, allowing more energy to dissipate through crack initiation and surface spalling. Stress occurs in the radial direction, creating a brittle-like failure with visible debris. The projectile flattens the impact zone, producing wide-area deformation and partial

material fracture. Tensile tension perpendicular to the plate's surface is the primary cause of radial cracks. This type of impact causes sudden failure with less plastic deformation, often simulating brittle behaviour even in ductile materials under high-strain-rate loading. Figure 18 depicts the failure mode and debris.

Conical Projectile

The conical projectile produces a highly localized stress concentration at the point of contact due to its sharp nose, which causes significant plastic deformation and necking around the impact site. The stress intensity initiates material flow radially outward, creating a conical crater. Necking is apparent as the material undergoes thinning before rupture. This projectile often penetrates deeply, with high-strain zones surrounding the entrance point. The large plastic zone represented ductile failure. The deformation profile implies significant material stretching, and the lack of a plug indicates gradual tearing rather than complete shear failure; however, all these deformations can be observed in Figure 19.

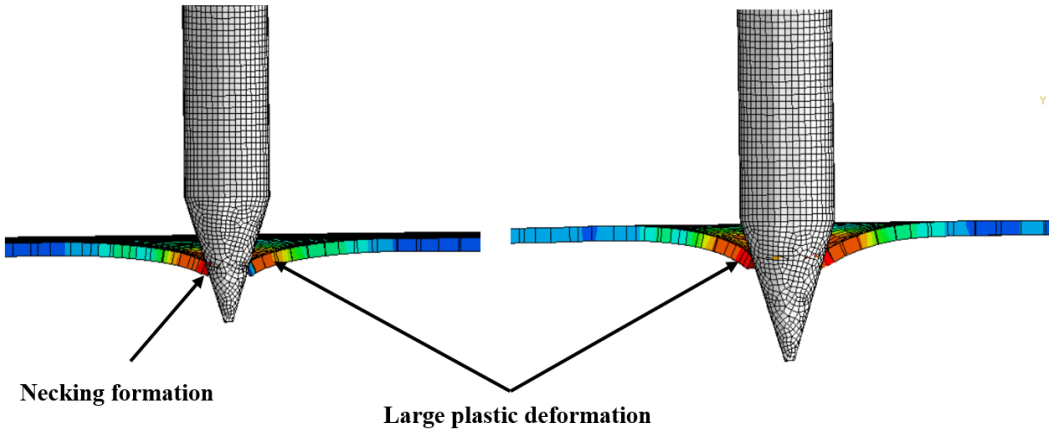

Figure 19. Simulation result for conical projectile after impact (Section view)

Spherical Projectile

The spherical projectile distributes stress over a larger surface compared to conical forms, resulting in lower peak stresses but wider deformation zones. The main failure mode is peeling, which happens when the plate bends and tears radially outward without ejecting a plug. This exhibits ductile response with modest plastic deformation. The impact causes out-of-plane bending, which results in radial crack growth. Petal generation absorbs significant energy, decreasing the penetration depth. The stress wave moves in a symmetrical pattern, efficiently transferring energy. Despite less penetration than pointed bullets, Figure 20 illustrates that the spherical nose creates a visually noticeable and structurally weakening deformation pattern around the impact location.

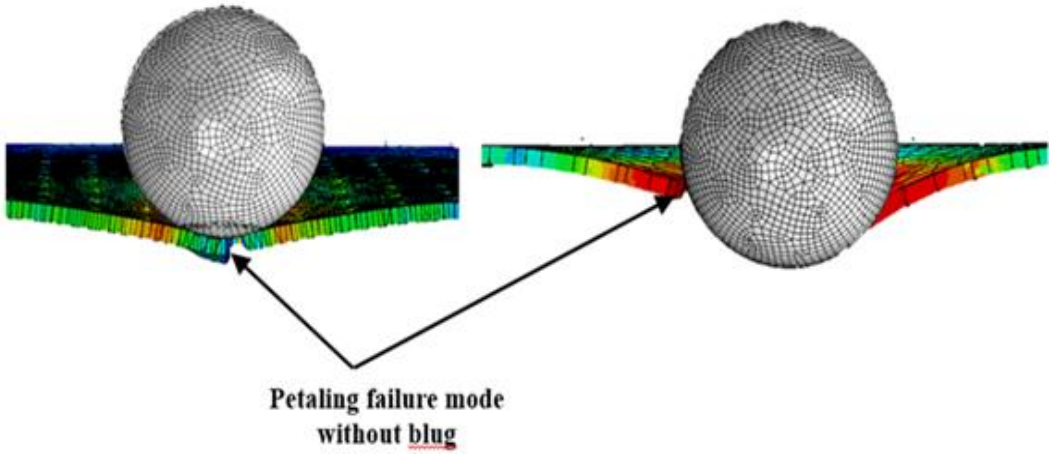

Figure 20. Simulation result for spherical projectile after impact (Section view)

Conclusions

Numerical models can effectively predict the effect of failure modes seen during experiments using the different nose shapes of projectiles. In the case of blunt projectiles, adiabatic shear band propagation is the failure mechanism that leads to plug ejection. Conical bullets cause the hole to expand and create a state of constant radial pressure. Depending on the impact velocity, the hemispherical projectile has pre-existing failure modes. Finally, a spherical projectile causes stress that is distributed over a larger area. The ballistic limit and the fracture time can be determined based on experimental findings for the majority of studies, with no significant variation between adaptive and fixed mesh. Numerical simulation convergence is the main distinction between these two techniques. One of the most considerable results of this study is that sharp-nosed conical projectiles are more effective for penetration because they retain greater velocities after impact, suggesting less energy absorption by the target. On the other hand, spherical and blunt-nosed projectiles are more effective at dissipating energy and causing surface or near-surface damage, which might be useful in certain applications, especially non-lethal impacts or energy absorption systems. In armor design, the choice of projectile to be tested must match the type of threat expected. For example, conical projectiles represent armor-piercing threats, while spherical projectiles represent blunt impact. Thus, knowing the interplay between projectile shape and target reaction is critical, particularly when constructing protective materials and structures to withstand various forms of kinetic energy threats. Furthermore, when subject to impact, the perforated plate has the same mechanical performance as the non-perforated plate. This property is essential because the perforated plate has a lower density while maintaining the same protective capacity.

Recommendations

A special premeditation can be reflected by several observations; hence, these points represent a substantial guide to developing the perforation plates as an important special type of armor:

- Altering the radius of perforations of the plate.
- Change the thickness of plates.
- Evaluating the performance of the system by using different types of projectiles' noses
- Replace the straight path of projectiles with an oblique path.
- Recommended to use new shapes of holes in the plate.

Scientific Ethics Declaration

* The authors declare that the scientific ethical and legal responsibility of this article published in EPSTEM journal belongs to the authors.

Conflict of Interest

* The authors declare no conflicts of interest.

Funding

* This study didn't receive any specific funds.

Acknowledgements or Notes

* This article was presented as an APA presentation at the International Conference on Engineering and Advanced Technology (ICEAT) held in Selangor, Malaysia on July 23-24, 2025.

* I declare that the research work entitled numerical analysis of perforation steel plates impacted by blunt, conical, hemispherical, and spherical projectiles, conducted by me under the supervision of Asst. Lect. Dr. Muhanad Hamed Mosa, was conducted strictly to the principles of scientific integrity and ethical conduct.

References

Alawsi, M. H. M., Al-Zobaede, A. M. A., & Al-Obaidi, S. M. A. (2025). Experimental and numerical study of ballistic impact performance on steel plate structures. *Journal of Engineering and Sustainable Development*, *29*(2), 177–183.

Alobaidi, H. A., & Almuramady, N. (2022). Influence of heat aging on tensile test in rubber-epoxy composites. *Al-Qadisiyah Journal for Engineering Sciences*, 132–135.

Alobaidi, H. A., & Almuramady, N. (2023). A review of fatigue analysis and mechanical approaches of rubber composites. *AIP Conference Proceedings*, *2787*(1).

Alobaidi, H. A., Almuramady, N., & Ali, M. M. (2023). Influence of adding epoxy on fatigue strength of natural rubber. *AIP Conference Proceedings*.

Arias, A., Rodríguez-Martínez, J., & Rusinek, A. (2008). Numerical simulations of impact behaviour of thin steel plates subjected to cylindrical, conical and hemispherical non-deformable projectiles. *Engineering Fracture Mechanics*, *75*(6), 1635–1656.

Ashaari, A. N., Kamarudin, K.-A., Nor, M. K. M., & Hatta, M. N. M. (2020). Numerical simulation on seashell structure subjected to impact using hemispherical and blunt projectiles. *Advanced Research in Natural Fibers*, *2*(2), 17–22.

Chen, C.-h., Zhu, X., Hou, H.-l., Tian, X.-b., & Shen, X.-l. (2017). A new analytical model for the low-velocity perforation of thin steel plates by hemispherical-nosed projectiles. *Defence Technology*, *13*(5), 327–337.

Chen, F., Peng, Y., Chen, X., Wang, K., Liu, Z., & Chen, C. (2021). Investigation of the ballistic performance of GFRP laminate under 150 m/s high-velocity impact: Simulation and experiment. *Polymers*, *13*(4), 604.

Chen, X., Peng, Y., Wang, K., Wang, X., Liu, Z., Huang, Z., & Zhang, H. (2023). Study on high-velocity impact perforation performance of CFRP laminates for rail vehicles: Experiment and simulation. *Biomimetics*, *8*(8), 568.

Coppinger, M. J., Wilmer, B. L., Adams, C. T., & Borys Jr, R. W. (2022). Electrified dynamic tensile extrusion of hemispherical nose aluminum projectiles.

Dubey, R., Jayaganthan, R., Ruan, D., & Velmurugan. (2021). Behavior of thermo-mechanically processed AA 6082 aluminium alloy impacted by conical projectiles. *Journal of Dynamic Behavior of Materials*, *7*, 48–59.

Ekrami, M., Ahmadi, H., Bayat, M., & Sabouri, H. J. (2017). Experimental study of projectiles with flat, conical and hemispherical nose shapes on low velocity impact on GLARE 3. *Modares Mechanical Engineering*, *17*(7), 109–118.

Ghazlan, A., Ngo, T., Tan, P., Tran, P., & Xie, Y. M. (2023). A numerical modelling framework for investigating the ballistic performance of bio-inspired body armours. *Biomimetics*, *8*(2), 195.

Hancock, J., & Mackenzie, A. (1976). On the mechanisms of ductile failure in high-strength steels subjected to multi-axial stress-states. *Journal of the Mechanics and Physics of Solids*, *24*(2-3), 147–160.

Ibrahim, M. N., Siswanto, W. A., & Zaidi, A. M. A. (2014). Numerical study on failure process of aluminium plate subjected to normal impact by hemispherical projectiles. *Applied Mechanics and Materials*, *660*, 598–602.

Mansour, M. Y., Mansour, M. H., Mostafa, N. H., & Rayan, M. A. (2016). Comparison study of supercavitation phenomena on different projectiles shapes in transient flow by CFD.

Mosa, M., Fahem, A., & Guthai, A. T. (2024). Experimental investigation of perforated multi-layered composite armor subjected to ballistic impact. *Al-Qadisiyah Journal for Engineering Sciences*, *17*(1), 16–21.

Mosa, M. H., & Hamza, M. N. (2022). Evaluating the performance of a unique design of biomimetic armor. *AIP Conference Proceedings*, *2415*(1).

Mosa, M. H., & Hamzah, M. N. (2022). Perforation resistance of four different thicknesses of AISI-1080 steel plates subjected to ballistic impact.

Oudah, A. A., Hassan, M. A., & Almuramady, N. (2023). Materials manufacturing processes: Feature and trends. *AIP Conference Proceedings*.

Reck, B., Alouahabi, F., Hassler, Q., & Schneider, M. (2022). Railgun launch of cylindrical and conical projectiles at muzzle velocities up to 2100 m/s. *Hypervelocity Impact Symposium*.

Rodríguez-Martínez, J. A., Rusinek, A., Pesci, R., & Zaera, R. (2013). Experimental and numerical analysis of the martensitic transformation in AISI 304 steel sheets subjected to perforation by conical and hemispherical projectiles. *International Journal of Solids and Structures*, *50*(2), 339–351.

Rusinek, A., Rodríguez-Martínez, J. A., Zaera, R., Klepaczko, J. R., Arias, A., & Sauvelet, C. (2009). Experimental and numerical study on the perforation process of mild steel sheets subjected to perpendicular impact by hemispherical projectiles. *International Journal of Impact Engineering*, *36*(4), 565–587.

Salimi, B., Vahedi, K., Petrudi, A. M., Rahmani, M., & Scurtu, I. C. (2022). Analytical study of the penetration of long rod projectiles with conical and blunt nose in normal and oblique ceramic targets. *Technium*, *4*(6), 35–49.

Senthil, K., Iqbal, M. A., Arindam, B., Mittal, R., & Gupta, N. (2018). Ballistic resistance of 2024 aluminium plates against hemispherical, sphere and blunt nose projectiles. *Thin-Walled Structures*, *126*, 94–105.

Sun, Y. S., Zhou, S. H., Zhang, X. B., & Xiang, Y. L. (2018). Study on the high-speed water impact load of hemispherical-nosed heavy projectiles. *Vibroengineering Procedia*, *17*, 137–141.

Tang, Y., & Li, D. (2022). Dynamic response of high-entropy alloys to ballistic impact. *Science Advances*, *8*(31), eabp9096.

Author(s) Information

Baneen Qasim Kazem
University of Al-Qadisiyah, Al-Diwaniyah, Iraq

Muhanad Hamed Mosa
University of Al-Qadisiyah, Al-Diwaniyah, Iraq
Contact e-mail: *muhanad.mosa@qu.edu.iq*

To cite this article:

Kazem, B. Q. & Mosa, M. H., & (2025). Numerical analysis of perforation steel plates impacted by blunt, conical, hemispherical, and spherical projectiles. *The Eurasia Proceedings of Science, Technology, Engineering and Mathematics (EPSTEM), 37,* 790-810.